Available online at www.sciencedirect.com
SCIENCE DIRECT®
Icarus 179 (2005) 415–431
ICARUS
www.elsevier.com/locate/icarus

Accretion of the gaseous envelope of Jupiter around a 5–10 Earth-mass core

Olenka Hubickyj [a,b,*], Peter Bodenheimer [a], Jack J. Lissauer [b]

[a] *UCO/Lick Observatory, Department of Astronomy and Astrophysics, University of California, Santa Cruz, CA 95064, USA*
[b] *Space Science Division, MS 245–3, NASA-Ames Research Center, Moffett Field, CA 94035, USA*

Received 13 January 2005; revised 18 June 2005

Available online 12 September 2005

Abstract

New numerical simulations of the formation and evolution of Jupiter are presented. The formation model assumes that first a solid core of several $M_\oplus$ accretes from the planetesimals in the protoplanetary disk, and then the core captures a massive gaseous envelope from the protoplanetary disk. Earlier studies of the core accretion–gas capture model [Pollack, J.B., Hubickyj, O., Bodenheimer, P., Lissauer, J.J., Podolak, M., Greenzweig, Y., 1996. Icarus 124, 62–85] demonstrated that it was possible for Jupiter to accrete with a solid core of 10–30 $M_\oplus$ in a total formation time comparable to the observed lifetime of protoplanetary disks. Recent interior models of Jupiter and Saturn that agree with all observational constraints suggest that Jupiter's core mass is 0–11 $M_\oplus$ and Saturn's is 9–22 $M_\oplus$ [Saumon, G., Guillot, T., 2004. Astrophys. J. 609, 1170–1180]. We have computed simulations of the growth of Jupiter using various values for the opacity produced by grains in the protoplanet's atmosphere and for the initial planetesimal surface density, $\sigma_{\mathrm{init},Z}$, in the protoplanetary disk. We also explore the implications of halting the solid accretion at selected core mass values during the protoplanet's growth. Halting planetesimal accretion at low core mass simulates the presence of a competing embryo, and decreasing the atmospheric opacity due to grains emulates the settling and coagulation of grains within the protoplanet's atmosphere. We examine the effects of adjusting these parameters to determine whether or not gas runaway can occur for small mass cores on a reasonable timescale. We compute four series of simulations with the latest version of our code, which contains updated equation of state and opacity tables as well as other improvements. Each series consists of a run without a cutoff in planetesimal accretion, plus up to three runs with a cutoff at a particular core mass. The first series of runs is computed with an atmospheric opacity due to grains (hereafter referred to as 'grain opacity') that is 2% of the interstellar value and $\sigma_{\mathrm{init},Z} = 10$ g/cm^2. Cutoff runs are computed for core masses of 10, 5, and 3 $M_\oplus$. The second series of Jupiter models is computed with the grain opacity at the full interstellar value and $\sigma_{\mathrm{init},Z} = 10$ g/cm^2. Cutoff runs are computed for core masses of 10 and 5 $M_\oplus$. The third series of runs is computed with the grain opacity at 2% of the interstellar value and $\sigma_{\mathrm{init},Z} = 6$ g/cm^2. One cutoff run is computed with a core mass of 5 $M_\oplus$. The final series consists of one run, without a cutoff, which is computed with a temperature dependent grain opacity (i.e., 2% of the interstellar value for $T < 350$ K ramping up to the full interstellar value for $T > 500$ K) and $\sigma_{\mathrm{init},Z} = 10$ g/cm^2. Our results demonstrate that reducing grain opacities results in formation times less than half of those for models computed with full interstellar grain opacity values. The reduction of opacity due to grains in the upper portion of the envelope with $T \leqslant 500$ K has the largest effect on the lowering of the formation time. If the accretion of planetesimals is not cut off prior to the accretion of gas, then decreasing the surface density of planetesimals lowers the final core mass of the protoplanet, but increases the formation timescale considerably. Finally, a core mass cutoff results in a reduction of the time needed for a protoplanet to evolve to the stage of runaway gas accretion, provided the cutoff mass is sufficiently large. The overall results indicate that, with reasonable parameters, it is possible that Jupiter formed at 5 AU via the core accretion process in 1 Myr with a core of 10 $M_\oplus$ or in 5 Myr with a core of 5 $M_\oplus$.
Published by Elsevier Inc.

* Corresponding author. Fax: +1 650 604 6779.
E-mail address: hubickyj@pollack.arc.nasa.gov (O. Hubickyj).

0019-1035/$ – see front matter Published by Elsevier Inc.
doi:10.1016/j.icarus.2005.06.021

Keywords: Jupiter, formation; Jupiter, interiors; Accretion; Origin of planetary systems

1. Introduction

Formation theories of our Solar System have entertained and challenged philosophers and scientists for centuries (Descartes, 1644; Kant, 1755; Laplace, 1796). Though it is agreed that the planets formed from high orbital angular momentum material left over from the formation of the Sun, the details of the process by which this remnant material creates the planets are still debated. There are two major models for the formation of the giant planets: the core accretion–gas capture model (alternatively referred to as the core accretion model) and the gas instability model. Core accretion (Perri and Cameron, 1974; Mizuno et al., 1978; Mizuno, 1980; Bodenheimer and Pollack, 1986, hereafter referred to as BP86) supposes that giant planets form in two stages: the formation of a massive solid core by coagulation of planetesimals in the solar nebula followed by the gravitational capture by the core of a massive envelope from the solar nebula gas. Gas instability is a single stage model in which the solar nebula becomes gravitationally unstable and rapidly collapses to form a gravitationally bound subcondensation known as a giant gaseous protoplanet (Kuiper, 1951; Cameron, 1978; DeCampli and Cameron, 1979; Boss, 1998, 2000, 2003; Mayer et al., 2002, 2004; Pickett et al., 2003; Rice et al., 2003a, 2003b). Evidence that all four giant planets within our Solar System have 10–15 $M_\oplus$ central cores made the core accretion model more popular in recent decades. The gas instability model never wholly disappeared and recent advances in the capabilities of multidimensional hydrodynamic simulations have revived interest in this model.

Any formation theory of giant planets in our Solar System needs to explain the observed bulk composition characteristics of these planets, namely, (1) the similarity in the total heavy element contents of Jupiter, Saturn, Uranus, and Neptune, (2) the very massive H_2 and He envelopes of Jupiter and Saturn and the much less massive (but nonnegligible) gaseous envelopes of Uranus and Neptune, and, (3) the general enhancement of metals over solar abundance in the atmospheres of all four giant planets (e.g., Pollack and Bodenheimer, 1989; Owen et al., 1999; Young, 2003). This enhancement is constrained and it cannot be larger than the total mass of heavy elements deduced to be in present Jupiter or Saturn, $\sim$25 $M_\oplus$, though there is a large possible uncertainty (Saumon and Guillot, 2004). Simulations based on the core accretion model have been successful in explaining these features of the giant planets (Pollack et al., 1996, hereafter referred to as Paper 1).

A major concern of the core accretion–gas capture model has been that the formation time for Jupiter in theoretical models with a minimum mass solar nebula is longer than observed disk lifetimes. The observational estimates of the lifetime of the disks around young stars are $\sim$0.1–10 Myr (Strom et al., 1993; Haisch et al., 2001; Chen and Kamp, 2004), and 3 Myr is the age at which half of the stars show evidence of disks. Initial Spitzer Space Telescope results (Bouwmann and Meyer, 2005) are consistent with these observed disk ages. Note, however, that these timescale estimates are based on thermal emission from small dust grains, not on observations of the gas. Evidently, these timescales vary from disk to disk and the distribution of their lifetimes is uncertain, too, but the upper limit on the lifetime of massive disks is generally quoted to be $<$10 Myr.

On the other hand, the giant gaseous protoplanets computed by Boss (1998), based on the gas instability model, are formed in $\sim 10^3$ yr, much less than the 1–50 Myr range reported in Paper 1. Although there are uncertainties in the processes of giant gaseous protoplanet formation, the disk instabilities are a dynamical effect, and if the planets could form by this process, they would do so very rapidly on timescales of at most a few tens of orbits. Though it was suggested by Boss (1998) that ice and rock cores *should* be able to form inside Jupiter after the occurrence of gravitational instability, there are no completed computations demonstrating this. Two basic requirements must be met for the disk instability to work: (1) the disk must be gravitationally unstable, and (2) the cooling time of the disk must be less than half an orbital period (Gammie, 2001). With regard to the first point, the gravitational stability of a Keplerian disk may be determined from the computed value of the Toomre Q parameter (Toomre, 1964); the disk is unstable for $Q \lesssim 1$. It remains to be shown that the collapse of a rotating presolar cloud results in a disk which has a Q value low enough for fragmentation. With regard to the second point, detailed radiation transfer calculations in a disk by Mejía et al. (2005) and Cai et al. (2004) indicate that the disk cooling time is too long to allow fragmentation to take place in the inner regions of disks. Boss (2004), on the other hand, showed that convection currents can bring energy out from the interior of a disk fast enough so that the cooling time requirement can be met outside a distance of about 8 AU. A recent study by Rafikov (2005) re-examined the conditions for planet formation by gas instability. Overall, he states that isothermal simulations should not be used to study planet formation in real protoplanetary disks and thermal conditions in the disk must be considered carefully. He determined that the cooling timescale ought to be comparable to the local disk orbital period. Interpreted into disk parameters, for planets to form at about 10 AU, the gas temperature of a disk with a mass of 0.7 $M_\odot$ and a luminosity of 40 $L_\odot$ should be $\sim 10^3$ K. These physical parameters are outside the generally observed range in protoplanetary disks.

The core accretion model and the gas instability model have been reviewed recently by Wuchterl et al. (2000) and

Bodenheimer and Lin (2002), and we need not repeat the details here. However, since we are using the core accretion model, we present a summary of its positive and negative aspects. The explanation for the bulk composition characteristics of the giant planets in our Solar System comes as a natural consequence of the core accretion scenario. The models in Paper 1 demonstrated that Jupiter and Saturn could reach the point of rapid gas accretion and form massive gaseous envelopes on timescales comparable to the lifetime of the solar nebula. The times for Uranus and Neptune to reach the point of rapid gas accretion were longer than the lifetime of the solar nebula, so they were unable to accrete a substantial envelope. The stream of planetesimals passing through and becoming dissolved in the envelope would explain the enhancement of metals over solar abundances in the atmospheres of the giant planets. However, these models were computed under idealized conditions of a lone embryo orbiting around the Sun with no planetesimal migration into or out of its feeding zone. Furthermore, to achieve an acceptably short formation time the surface density of solid material in the disk was presumed to be about 3 times higher than that of the minimum mass solar nebula having a surface density of 3 g/cm^2 at 5 AU. According to the minimum mass solar nebula model of Weidenschilling (1977), this quantity can vary between 1.7 and 34 g/cm^2 at Jupiter's position. The upper limit on the minimum mass solar nebula should now be revised to 8 g/cm^2, based on the upper limit to Jupiter's heavy-element mass (Saumon and Guillot, 2004). The calculated core masses for Jupiter (Paper 1) were generally about 20 $M_\oplus$, which is higher than the more recently deduced upper limit from the interior model calculations based on observable data (Saumon and Guillot, 2004).

With regard to the growing number of extrasolar planets, it is well established observationally that the planet occurrence rate is positively correlated with the metal abundance of the host star (Gonzalez, 1998; Santos et al., 2001, 2004; Fischer and Valenti, 2003, 2005). While this trend has been found to be consistent with simplified core accretion models (Ida and Lin, 2004; Kornet et al., 2005), it has also been suggested (Sigurdsson et al., 2003) that the correlation is a result of preferential migration of planets in high-metallicity disks into the period range where they are observed. Sozzetti (2004) suggests that there is a correlation between observed orbital period and the host star metallicity in the sense that the higher-metallicity stars are more likely to have short-period planets. This tendency would be consistent with the migration scenario; however, the correlation is weak, and Santos et al. (2003) do not find it. On the theoretical side, the simple model of Livio and Pringle (2003) results in only a small difference in migration rates in metal-rich and metal-poor disks, not sufficient to explain the trend seen in Fischer and Valenti (2005). Thus, this correlation is more likely to be a result of the formation mechanism itself. Although a higher-metallicity planet has a higher opacity in the envelope, which results in longer formation times (see below), increases in opacity by only a factor of 2 have a very small effect on the time.

A substantial amount of information about the interior structure of Jupiter, including evidence of the presence of a solid core, is extracted when structure model parameters (mass, radius, gravitational moments) are matched with the observed values (Pollack, 1985; Marley, 1999). Recent interior models of Jupiter and Saturn that agree with all observational constraints show that Jupiter's core mass is at most 11 $M_\oplus$ and Saturn's is between 9–22 $M_\oplus$ (Saumon and Guillot, 2004). The wide range of possible core masses is a consequence of uncertainties in the equation of state of a mixture of hydrogen and helium at megabar pressures. If one restricts the choice of equations of state to those which agree with available experimental data, the range of possible core masses for Jupiter is 0–3 $M_\oplus$ and for Saturn is 12–21 $M_\oplus$ (Guillot, 2005, his Fig. 7).

Simulations of the accumulation of jovian planets complement the theoretical structure models, and the integration of the results of both types of calculations with observational constraints on formation timescales provides the means to explore mechanisms by which the planets were formed. Calculations of the growth of Jupiter (Mizuno et al., 1978; Mizuno, 1980; BP86, Paper 1) report solid core masses ranging from 10 to 35 $M_\oplus$. The problem is that the lower core masses in those calculations correspond to longer evolutionary times; in particular, according to calculations with the standard parameters in Paper 1 (case J2), a planet with a core mass of 11 $M_\oplus$ would take ~50 Myr to form, which is much longer than observed disk lifetimes. Giant planet formation can proceed more rapidly either in a more massive protoplanetary disk (Paper 1) or in a given disk if the planet migrates relative to the planetesimals, thereby accessing accretable material in undepleted regions of the disk (Alibert et al., 2004, 2005). With a solid surface density at 5 AU equal to that of case J2 in Paper 1 (i.e., 7.5 g/cm^2), they find, for a parameterized choice of migration rate (0.01 to 0.1 times that given by Tanaka et al., 2002), that Jupiter forms in 1–2.2 Myr with a total heavy element abundance still consistent with observations (albeit near the upper end of the large error bars). However, in their model all this mass is assumed to be in the core, so the low-core-mass problem is still unsolved. Similar conclusions are reached by Rice and Armitage (2003), who modeled the accretion of Jupiter including migration according to a random walk in a turbulent disk. By reducing the solid surface density to 5 g/cm^2, they get runaway gas accretion after 1.5 Myr and a core mass of 6 $M_\oplus$, but do not match the total heavy element abundance of Jupiter. Thus, migration with arbitrary parameter choices makes it possible to form Jupiter in 1–2 Myr starting from a disk with lower solid surface density, closer to the minimum mass solar nebula, than that needed for nonmigrating models. However, these models still do not satisfy the constraints on heavy element abundances (Saumon and Guillot, 2004). Thus this process only speeds growth for fixed disk properties, not fixed heavy element abundances, which are

the observationally-constrained data for planets within our Solar System.

In light of the interior models that suggest lower solid core masses than those predicted in Paper 1, the new challenge to the core accretion model is to demonstrate that even a protoplanet with a low mass core can capture a gas envelope that can grow to present day Jupiter's mass on a timescale consistent with disk observations. It may be necessary to assume that the planet actually formed with a 10–25 $M_\oplus$ core, which was later eroded by convective mixing and its material dissolved into the envelope (Stevenson, 1982; Guillot, 2001; Guillot et al., 2004). Alternatively, Ikoma et al., 2000 (hereafter referred to as INE00) examined the dependence of the formation time on various core accretion rates and atmospheric opacity values. Their models were computed using a hydrostatic envelope structure and a quasi-static evolution with similar assumptions to those in Paper 1. However, unlike the models in Paper 1, the core accretion rate is constant and is regarded as a parameter. The opacity due to grains is also a parameter and it is set to various constant values (10^{-4}, 10^{-2}, 10^{-1}, and 1 cm^2/g) in the region of the envelope where the temperature is less than 1800 K, the vaporization temperature of the most refractory grains. An important result of the INE00 study is that a solid core of any small size can capture nebular gas *if* the grain opacity is small enough. However, the accretion time for the gas becomes longer when the core mass is decreased. This implies that there is a minimum value for the core mass which INE00 found to be $M_{\rm core,min} \sim 5\ M_\oplus$, for which the protoplanet is unable to capture enough of the solar nebula gas within the lifetime of the solar nebula to make a giant gaseous planet. A related calculation (Papaloizou and Nelson, 2005) treats the gas accretion phase with fixed core mass and no solid accretion. Gas accretion times, not including core formation times, are 3×10^8 and 3×10^6 yr for a 5 $M_\oplus$ core and with interstellar and 1% interstellar grain opacity, respectively. If the core mass is increased to 15 $M_\oplus$, the corresponding times are 3×10^6 and $\sim 10^5$ yr, respectively.

In the present study, we compute simulations of the growth of Jupiter using the core accretion–gas capture model. Our simulations use various different values of the atmospheric opacity at temperatures $T < 1800$ K, where grains make a substantial contribution to the Rosseland mean opacity. This parameter was shown in Paper 1 to have substantial effect on the formation timescale. We also vary the planetesimal surface density in the solar nebula, which Paper 1 found to influence the final core mass of the planet, and explore the implications of halting the solid accretion at selected core mass values during the protoplanet's growth. The goal of the calculations is to answer the question: Can a giant planet with a core mass of 10 $M_\oplus$ or less be produced on a timescale of a few Myr?

In most of the simulations presented in Paper 1 the protoplanet builds up as an isolated embryo and there are no other embryos that compete for planetesimals. Here we relax the assumption of the lone embryo by cutting off the solid accretion entirely once the core mass has reached some prescribed value, thereby approximately simulating the influence of neighboring embryos. The results show that, depending on the mass of the core, the evolutionary timescale can be increased or decreased. Preliminary results on such cutoff calculations were reported in Paper 1, and the problem was further explored by INE00.

Standard interstellar grain properties were used in the calculations in BP86 and in Paper 1. Those opacities were based on a solar mixture of elements with the grains having an interstellar size distribution (with typical size less than a few tens of microns). Discussions of the validity of applying opacities based on this solar mixture to giant planet envelopes appear in Paper 1 and INE00. The main point is that the grain properties in the material that enters a giant planet envelope over a period of several Myr have been strongly modified from the original interstellar grains by coagulation and fragmentation and by settling to the midplane of the disk. Thus, it is difficult to estimate the actual grain opacities, even if the grains did not settle after arriving in the outer envelope (Lissauer et al., 1995). Calculations by Podolak (2003) indicate that once the grains enter the protoplanetary envelope, they coagulate and settle out quickly into warmer regions where they are destroyed, so actual opacities at low temperatures are far less than interstellar values. Podolak's results imply that the standard opacities in models from Paper 1 were too high in the grain region. Reduced opacities in the outer parts of the protoplanet have the effect of reducing the timescale (e.g., model J6 in Paper 1), but they do not influence the final core masses. Thus, we define a baseline case using a grain opacity reduced to 2% of the interstellar value, and then compare it with a model using the full interstellar opacity.

The final parameter to be examined is the surface density of planetesimals. Lissauer (1987) showed that in order to get reasonable core formation times this quantity must be enhanced over that in the minimum mass solar nebula by a factor of several. Detailed numerical simulations (Paper 1, INE00) indicate that the factor is probably in the range 3–4, although more recent detailed calculations of the core accretion process (Inaba et al., 2003) indicate that the required factor is larger, in the range 4–8. The standard value assumed here, for a proto-Jupiter at 5 AU, is 10 g/cm^2, which is about 3 times that in the minimum mass solar nebula. Models were computed with the solid surface density reduced to 6 g/cm^2. The models in Paper 1 show that decreasing the surface density of planetesimals can cause the formation timescale to be significantly extended; however, reducing it has the desirable effect of lowering the final core mass of the protoplanet.

The core accretion model, the computer program, and the modifications and updates made to the code are described in Section 2. The results are presented in Section 3. A discussion of the results and the presentation of conclusions in Section 4 completes this paper.

2. Procedure

Our code consists of three main components: (1) the calculation of the rate of solid planetesimal accretion by the protoplanet; (2) the calculation of the interaction of the accreted planetesimals with the gas in the envelope; and (3) the calculation of the gas accretion rate and thermal evolution of the protoplanet. Since Paper 1 was published, we have made changes and updates to the code simulating the formation process, some of which are described in Bodenheimer et al., 2000 (hereafter referred to as BHL00). A full, detailed, description of the computational protocol is in Paper 1, but we present here a comprehensive review and summary of the present state of the computer code and the associated assumptions.

As described in BHL00, the evolution of the giant protoplanet is viewed to occur in the following sequence: (1) Dust particles in the solar nebula form planetesimals that accrete, resulting in a solid core surrounded by a low mass gaseous envelope. Initially, solid runaway accretion occurs, and the gas accretion rate is much slower than that of solids. As the solid material in the feeding zone is depleted, the solid accretion rate is reduced. The gas accretion rate steadily increases and eventually exceeds the solid accretion rate. (2) The protoplanet continues to grow as the gas accretes at a relatively constant rate. The mass of the solid core also increases but at a slower rate. Eventually, the core and envelope masses become equal. (3) Near this point, the rate of gas accretion increases in runaway fashion, and the protoplanet grows at a rapidly accelerating rate. The first three parts of the evolutionary sequence are referred to as the *nebular* stage, because the outer boundary of the protoplanetary envelope is in contact with the solar nebula, and the density and temperature at this interface are those of the nebula. (4) The gas accretion rate reaches a limiting value defined by the rate at which the nebula can transport gas to the vicinity of the planet. After this point, the equilibrium region of the protoplanet contracts inside the effective accretion radius (defined in BHL00), and gas accretes hydrodynamically onto this equilibrium region. This part of the evolution is considered to be the *transition* stage. (5) Accretion is stopped by either the opening of a gap in the disk as a consequence of the tidal effect of the planet, accumulation of all nearby gas, or by dissipation of the nebula. Once accretion stops, the planet enters the *isolation* stage. (6) The planet contracts and cools to the present state at constant mass.

The first component of the code computes the solid accretion rate, $\dot{M}_Z$. It is assumed that a single, dominant mass resulted from a runaway growth in a swarm of planetesimals orbiting around the Sun (Greenberg et al., 1978; Weidenschilling et al., 1997). We apply an updated version (Greenzweig and Lissauer, 1992) of the classical theory of planetary growth (Safronov, 1969) to calculate $\dot{M}_Z$:

$$\dot{M}_Z = \pi R_{\text{capt}}^2 \sigma_Z \Omega F_g, \tag{1}$$

where R_{capt} is the effective (geometric) capture radius of the protoplanet for a planetesimal of a given size, σ_Z is the surface density of solid planetesimals in the solar nebula, Ω is the orbital frequency, and F_g is the gravitational enhancement factor, which is the ratio of the total effective accretion cross section to the geometric cross section. Greenzweig and Lissauer (1992) have computed F_g; their calculation consists of a large number of three-body (Sun, protoplanet, and planetesimal) orbital interaction simulations, where the planetesimals have a Rayleigh distribution in eccentricities and inclinations. We use an analytical expression for F_g (Greenzweig and Lissauer, 1992) that was derived to fit the data from the numerical calculations. We assume that the growing protoplanet is surrounded by a disk with an initially uniform surface density in the region of the protoplanet, $\sigma_{\text{init},Z}$, consisting of planetesimals with the same mass (m_p) and radius (r_p). The protoplanet's feeding zone is assumed to be an annulus extending to a radial distance of about 4 Hill-sphere radii on either side of its orbit (Kary and Lissauer, 1994). The feeding zone grows as the planet gains mass, and random scattering is assumed to spread the unaccreted planetesimals uniformly over the feeding zone. Radial migration of planetesimals into and out of the feeding zone is not considered. However, the effects of radial migration of planetesimals, the planetesimal size distribution, and fragmentation can have significant consequences for giant planet growth (Inaba et al., 2003). These effects will be incorporated in future calculations.

The second component of the code computes the interaction of the planetesimals with the envelope of the protoplanet, and determines whether the planetesimals reach the core, or are dissolved in the envelope, or a combination of the two. Calculations of trajectories of planetesimals through the envelope (Podolak et al., 1988, Paper 1) result in: (1) the radius in the envelope, R_{capt}, at which the planetesimal is captured, which is required to compute the accretion rate of the planetesimals (first component), and (2) the energy deposition profile in the envelope, which is required for the structure computation (third component). To evaluate the velocity of the planetesimal at the outer boundary of the protoplanet (R_p), an analytic solution to the two-body (protoplanet and planetesimal) problem with no gas drag is obtained. Once inside the protoplanetary envelope, the planetesimal's trajectory is computed for a particular impact parameter using a numerical integration (4th order Runge–Kutta) scheme of the equations of motion influenced by the gravitational field of the core and envelope as well as gas drag. The trajectory calculation is repeated for a series of 20 impact parameters ranging from zero to the critical impact parameter inside of which the planetesimal is captured. The planetesimal is considered captured when it displaces an amount of gaseous matter comparable to its own mass (see Paper 1). In the early part of the evolution, a planetesimal traversing the low mass gaseous atmosphere reaches the core almost intact. At later stages, when the protoplanet has a higher mass envelope, material is ablated from the planetes-

imal into the envelope, and substantial amounts of mass and energy are deposited. We amended the capture criterion used in Paper 1 to include planetesimals that deposit 50% or more of their mass into the envelope during their trajectory. The planetesimals and debris ablated therefrom are assumed to sink to the core, liberating additional energy in the process. This is a simplification, as some components of the planetesimals, once vaporized in the envelope, are likely to remain dissolved there. However, detailed calculations of the equation of state and solubility are required to take this effect into account.

The third component of our code computes the structure and the evolution of the envelope by means of a series of quasi-equilibrium models. The conventional stellar structure equations of conservation of mass and energy, hydrostatic equilibrium, and radiative or convective energy transport are used. Application of the hydrostatic equilibrium condition to the envelope models has been justified by Tajima and Nakagawa (1997), particularly in the case of the models with a constant solid accretion rate. The energy generation rate is the result of the accretion of planetesimals and the quasi-static contraction of the envelope. In the earliest part of the evolution, when the planetesimals land directly on the core, the deposited energy is smeared, for numerical reasons, over a region of about one-core radius. The equation of state is nonideal and has been updated since Paper 1 to tables based on the calculations of Saumon et al. (1995), interpolated to a near-protosolar composition of $X = 0.74$, $Y = 0.243$, $Z = 0.017$. The opacity tables are derived from the calculations of Pollack et al. (1985) as well as those of Alexander and Ferguson (1994), which were not available for the calculations in Paper 1. As discussed in the Introduction, the grain opacities in these tables are based on an interstellar size distribution. The grain opacities are modified in some runs. The outer boundary of the protoplanet, during the nebular stage, is defined to be the effective accretion radius R_a, outside of which gas is not gravitationally bound to the protoplanet (cf. BHL00). Gas accretion occurs when the outer envelope contracts and when R_a increases as the planet's total mass increases. It is assumed that gas from the surrounding solar nebula flows freely into the evacuated volume at the rate $\dot{M}_{XY}$ needed to restore the condition $R_p = R_a$.

The calculations start at $t = 10^4$ yr with a core mass of 0.1 $M_\oplus$ and an envelope mass of 10^{-9} $M_\oplus$. These initial values were chosen for computational convenience and the final results are insensitive to moderate changes in these initial conditions. The inner and outer boundary conditions are set at the bottom and top of the envelope, respectively. At the inner edge, the luminosity, $L_r = 0$ and $r = R_{\rm core}$, where $R_{\rm core}$ is determined from the current core mass M_Z and the core density $\rho_{\rm core}$, which is assumed to be constant at 3.2 g/cm^3. At the outer edge during the nebular stage, the density ($\rho_{\rm neb}$) and temperature ($T_{\rm neb}$) are fixed and obtained from standard disk models. The models in Paper 1 were computed until the evolution passed *crossover* mass ($M_{\rm cross}$, the mass at which the accreted solid mass equals the accreted gas mass) and $\dot{M}_{XY}$ was a factor of 10 greater than $\dot{M}_Z$. This criterion was chosen for numerical convenience since our prime objective was to examine the planetary growth through the initial phase of the gas runaway stage of formation. Changes have been made to the code to extend the calculation through the cooling and contraction phase after the solar nebula has dissipated (BHL00), and all four models without planetesimal accretion cutoff are computed through this phase. The simulations for the cutoff models are terminated when the gas accretion rate has reached its limiting value, and thus the formation time has been well established. The limiting gas accretion rate is determined by the ability of the solar nebula to supply gas at the required rate. In a typical model of a protoplanetary nebula, the mass transfer rate at a given radius, caused by viscous effects, is 3×10^{-8} $M_\odot$/yr (equivalent to 10^{-2} $M_\oplus$/yr). When this limiting rate is reached, the planet contracts inside R_a, and the evolution enters the transition stage. The planet is still assumed to be in hydrostatic equilibrium, but gas is accreting hydrodynamically onto it at near free-fall velocities. The details of how the boundary condition is applied to the equilibrium planet are described in BHL00. The assumption of spherical symmetry is made here, but in fact the flow of gas at this stage will be rotationally dominated, and accretion will occur through a circumplanetary disk. Two- and three-dimensional simulations (Kley, 1999; Kley et al., 2001; D'Angelo et al., 2003) show that accretion onto the planet does take place at the rate at which the main disk feeds gas into the planet's Hill sphere. For a standard viscosity, this rate is 10^{-8}–10^{-7} $M_\oplus$/yr, consistent with our assumption.

The supply of gas to the planet is eventually assumed to be exhausted (e.g., as a result of tidal truncation of the nebula, removal of the gas by effects of the star, and/or the accretion of all nearby gas by the planet). In fact, gap opening (tidal truncation) should start before a Jupiter mass is reached, but it does not necessarily stop accretion onto the planet (Bryden et al., 1999; Kley, 1999; Lubow et al., 1999; Nelson et al., 2000). Simulations have shown that a planet can still grow to several Jupiter masses. But here we simply assume that there has been sufficient dispersal of disk material (Hollenbach et al., 2000) so that the final mass levels off at 1 Jupiter mass. This process is not modeled in detail, but $\dot{M}_{XY}$ onto the planet is assumed to reduce smoothly to zero as the limiting value is approached. The planet then evolves through the isolation stage, during which it remains at constant mass. The boundary conditions are then simply the standard photospheric conditions

$$L = 4\pi\sigma_{\rm SB} R_p^2 T_{\rm surf}^4, \tag{2}$$

where $\sigma_{\rm SB}$ is the Stefan–Boltzman constant, and

$$\kappa P = \frac{2}{3} g, \tag{3}$$

where P and κ are the photospheric pressure and Rosseland mean opacity, respectively, and g is the acceleration of gravity at R_p.

The effect of the new physics that we have included are illustrated by comparing our new case 10H$^{\infty}$ (notation is explained in Section 3) to the Jupiter baseline case in Paper 1 (case J1). Comparison of these two models show there is a difference in crossover times: $t_{\rm cross} = 7.58 \times 10^6$ yr for J1 and 6.07×10^6 yr for 10H$^{\infty}$, and with no difference in $M_{\rm cross}$. We determined that the application of the new equation of state of Saumon et al. (1995) (which causes the timescales to increase) and the opacity tables of Alexander and Ferguson (1994) (which causes the timescales to decrease) to the evolution code accounts for most of the difference in formation times between the two Jupiter calculations. The other changes made in the code that were discussed in Section 2 (i.e., modifying the criterion for planetesimal capture, changing the outer boundary of the envelope, and installing a distribution of impact parameters for the incoming planetesimals) made very small contributions. To determine exactly what contributed to the differences between J1 and 10H$^{\infty}$, we used the original version of the code that calculated the models in Paper 1 and made table substitutions in a step-wise manner. First, the opacity tables used in Paper 1 (Alexander, 1975; Alexander et al., 1983; Cox and Stewart, 1970) were replaced with those of the updated tables of Alexander and Ferguson (1994) but the opacity table for the low T region (Pollack et al., 1985) was retained. The crossover time for this model is 4.80×10^6 yr, quite a bit less than the 7.58×10^6 yr of the J1 model. The second run was computed with the old opacity tables but with the new equation of state tables (Saumon et al., 1995, rather than the old Graboske et al., 1975; Grossman et al., 1980), which resulted in a crossover time of 10.38×10^6 yr, quite a bit longer than that of J1. The final run was computed with the new opacity and new equation of state tables. The crossover time is 6.11×10^6 yr, less than in J1 but in agreement with our updated version, 10H$^{\infty}$, 6.07×10^6 yr. The remaining discrepancy in $t_{\rm cross}$ between 10H$^{\infty}$ and J1 (about 0.04×10^6 yr) is attributed to the other changes made to the code. $M_{\rm cross}$ for all of these runs was 16.16 $M_{\oplus}$, the same as for J1.

Table 1 lists the parameters and nominal values used in the Jupiter simulations presented herein as well as the properties of the planetesimals being accreted by the protoplanet. The planetesimal properties are the same as those used in Paper 1 and in BHL00.

Table 1
Model parameters and nominal values

Parameter	Nominal value
Orbital distance	5.2 AU
Planetesimal radius	100 km
Initial planetesimal surface density	10 g/cm^2
Fate of dissolved planetesimal	Sinks to core interface
Nebula temperature	150 K
Nebula density	5.0×10^{-11} g/cm^3

Properties of planetesimals

Property	Component[a]			
	H_2O ice	Rock	CHON	Total
Mass fraction	0.397	0.308	0.295	1
Density (g/cm^3)	0.92	3.45	1.5	1.39
Latent heat[b] (erg/g)	2.8×10^{10} [c]	8.08×10^{10} [c]	-7.0×10^{10} [d]	1.54×10^{10}
Vaporization temperature (K)	165	1500	650	–

[a] The three major components of the planetesimals are water ice, ferromagnesium silicates ('rock'), and organics ('CHON').
[b] The latent heats of ice and rock are endothermic, while that of the CHON is exothermic.
[c] Podolak et al. (1988).
[d] Estimated.

3. Results

We present the results of our Jupiter formation simulations. As discussed in Section 1, our goal was to compute models for Jupiter with low mass cores (Guillot et al., 1997; Wuchterl et al., 2000; Saumon and Guillot, 2004) that will form within the dissipation timescale limit of the solar nebula. The results of Paper 1 demonstrated that reducing the grain opacity decreases the time for the protoplanet to evolve to crossover, yet $M_{\rm cross}$ is unchanged. It was also shown that if the planetesimal surface density is reduced, $M_{\rm cross}$ decreases but at the expense of increasing the evolution time. Simulations were computed in Paper 1 (J1a, J1b, J1c) with the core accretion turned off at selected times. These models showed that the evolutionary timescale was affected by such a cutoff. In all three cases, the time to crossover was shorter than in the case with no core accretion cutoff, and the run with the shortest time to crossover had solid accretion cutoff occur soon after the runaway solid accretion caused a significant depletion of planetesimals in the effective feeding zone of the protoplanet. Based on these results we examine the sensitivity of giant planet growth to the following three main parameters: the atmospheric opacity due to grains, the surface density of solids in the disk, and the core mass at which solid accretion is turned off.

The baseline case is an evolution of Jupiter progressing through the (1) nebular, (2) transition, and (3) isolation stages. It was computed with the planetesimal surface density, $\sigma_{{\rm init},Z} = 10$ g/cm^2, the grain opacity at 2% of the interstellar value, and no core accretion cutoff. Another evolution case is computed with the same planetesimal surface density, but the grain opacity is set to the full interstellar value. A third run is computed with a "variable" grain opacity in the envelope: for temperatures <350 K the grain opacity is 2% interstellar, linearly increasing (relative to interstellar) opacity for $350 \leqslant T \leqslant 500$ K, and for temperatures >500 K the grain opacity is set to the full interstellar value. This run crudely mimics an upper envelope depleted of grains due to settling processes that were investigated by Podolak (2003). Another simulation is computed using $\sigma_{{\rm init},Z} = 6$ g/cm^2 and the grain opacity at 2% interstellar. To approximate the effect of nearby developing embryos that are competing for

Table 2
Input parameters

Case	$M_{\rm cutoff}$ ($M_\oplus$)	$\kappa_{\rm gr}$	$\sigma_{{\rm init},Z}$ (g/cm^2)	σ_{XY} (g/cm^2)
10L$^\infty$	–	2% interstellar	10	700
10L10	10	2% interstellar	10	700
10L5	5	2% interstellar	10	700
10L3	3	2% interstellar	10	700
10H$^\infty$	–	Interstellar	10	700
10H10	10	Interstellar	10	700
10H5	5	Interstellar	10	700
6L$^\infty$	–	2% interstellar	6	420
6L5	5	2% interstellar	6	420
10V$^\infty$	–	2% interstellar ($T < 350$ K) Interstellar ($1800 > T > 500$ K)	10	700

the nebular solid and gas material, some of these models are recomputed with the planetesimal accretion stopped at core masses chosen to be 10, 5, and 3 $M_\oplus$. Table 2 lists the parameters of all the computer simulations, denoting the grain opacity value, the surface density, and the core mass at which the solid accretion is turned off.

We have adopted a nomenclature for our simulations that illustrates the parameters used in the computations. The form is: σ–opacity–cut, where σ is the initial surface density of planetesimals in the solar nebula with values 10 or 6 g/cm^2; *opacity* is denoted by either "L" for grain opacity at 2% of the interstellar value, "H" for the full interstellar value, and "V" for a variable (temperature dependent) ratio of opacity to the interstellar value; and *cut* specifies the core mass (in units of $M_\oplus$) at which the planetesimal accretion rate is turned off. For cases with no solid accretion cutoff, *cut* is set to ∞. As an example, the model labeled 10L$^\infty$ (the baseline case) signifies that the simulation was computed with $\sigma_{{\rm init},Z} = 10$ g/cm^2, the grain opacity is 2% of the interstellar value and there was no solid accretion cutoff.

Table 3 summarizes the results of all of the simulations, listing the time, mass, accretion rates, and luminosity values at five salient milestones during the evolution: (1) the first maximum of the luminosity during rapid solid accretion, (2) the end of Phase 1, defined when $\dot{M}_Z = \dot{M}_{XY}$ for the ∞ cases and *just* prior to solid accretion cutoff for the runs in which $\dot{M}_Z > \dot{M}_{XY}$ at all times prior to cutoff, (3) mid-Phase 2, defined as when $M_{XY} = 0.5\ M_Z$, (4) the crossover point, defined when $M_Z = M_{XY}$, and, finally, (5) the onset of limiting gas accretion, $\dot{M}_{XY} = 10^{-2}\ M_\oplus$/yr. A simple average over a set number of (about a dozen) consecutive points was performed on the luminosity, $\dot{M}_{XY}$, and $\dot{M}_Z$ in order to minimize the numerical noise.

Fig. 1 plots the masses, luminosity, accretion rates, and radii as a function of time for the evolution of the Jupiter model 10L$^\infty$. These plots (particularly, Figs. 1a and 1c) clearly show the three distinct characteristic phases of the protoplanet evolution in the nebular stage: the rapid solid mass accretion followed by the decrease in the rate as the solid material in the feeding zone is depleted of planetesimals (Phase 1), the settling into a steady state where the gas accretion rate exceeds the solid accretion rate (Phase 2), and, then, the increase in gas mass to crossover which leads into gas runaway (Phase 3). Phase 1 lasts for 0.38×10^6 yr, the maximum solid accretion rate is $9.0 \times 10^{-5}\ M_\oplus$/yr, and the luminosity peaks at $\log(L/L_\odot) = -5.05$. The isolation mass, defined as the mass of the protoplanet after it has depleted its feeding zone (Lissauer, 1987), is expressed as

$$M_{\rm iso} = C_1 (a^2 \sigma_{\rm init})^{3/2}, \tag{4}$$

where $C_1 = 1.56 \times 10^{25}$ g if $\sigma_{\rm init}$ is in units of g/cm^2 and a is in units of AU. The computed isolation mass is $M_Z = 11.5\ M_\oplus$ for model 10L$^\infty$ (Table 3), which is in good agreement with the analytic value of 11.56 $M_\oplus$. The mass of the envelope at the end of Phase 1 is 0.31 $M_\oplus$. During the first half of Phase 1, $R_{\rm capt}$ and $R_{\rm core}$ are very nearly the same, as shown in Fig. 1d, because the envelope is not very massive, and, therefore, the planetesimals either hit the core or break apart very near the core. For this model, $R_{\rm capt}$ and $R_{\rm core}$ separate at about $t_{\rm evol} = 0.18 \times 10^6$ yr, which occurs before the solid accretion rate maximum at $t_{\rm evol} = 0.28 \times 10^6$ yr and $M_Z = 7\ M_\oplus$. From the time these two radii begin to diverge, $R_{\rm core}$ settles to a value of about 0.25 R_J at the end of Phase 1, increasing slightly to 0.28 R_J at $t_{\rm cross}$. Over the same period of time, $R_{\rm capt}$ increases to a value of 7 R_J, about 30 time larger than $R_{\rm core}$. Figs. 1a and 1c clearly illustrate Phase 2, which lasts for 1.84×10^6 yr. Crossover occurs at $t_{\rm cross} = 2.22 \times 10^6$ yr, which is considerably shorter than $t_{\rm cross} = 7.58 \times 10^6$ yr for the baseline Jupiter model, J1, in Paper 1. However, $M_{\rm cross} = 16.08\ M_\oplus$ is only slightly smaller than $M_{\rm cross} = 16.16\ M_\oplus$ for J1. The major factor causing the difference in the formation time is the grain opacity in the envelope.[1]

For the four simulations without solid accretion cutoff, the mass and luminosity as a function of time are plotted in Figs. 2a and 2b, respectively. The changes due to grain opacity differences (models 10L$^\infty$, 10V$^\infty$, and 10H$^\infty$) and $\sigma_{{\rm init},Z}$ (models 10L$^\infty$ and 6L$^\infty$) are evident. For all the models with $\sigma_{{\rm init},Z} = 10$ g/cm^2, Phase 1 is similar in duration, spanning 3.8×10^5 and 4.5×10^5 yr for cases 10L$^\infty$ and 10H$^\infty$, respectively. Phase 1 for 6L$^\infty$ lasts for 6.5×10^5 yr, which, as expected, is longer than the higher $\sigma_{{\rm init},Z}$ cases. Since the solid surface density of planetesimals is lower in 6L$^\infty$, the rate of accretion, $\dot{M}_{Z,\max} = 1.95 \times 10^{-5}\ M_\oplus$/yr, is lower by almost a factor of 5 as compared with 10L$^\infty$. The luminosity at the peak of solid accretion is similar for models 10L$^\infty$ and 10H$^\infty$, $\log(L/L_\odot) = -5.085$ and -5.17,

[1] Model 10L$^\infty$ is an updated calculation of case J6 of Paper 1. There is a small difference of timescales between these two models: $t_{\rm cross} = 2.75 \times 10^6$ yr for J6 and $t_{\rm cross} = 2.22 \times 10^6$ yr for 10L$^\infty$, with a slight difference in $M_{\rm cross}$: 16.18 $M_\oplus$ for J6 and 16.08 $M_\oplus$ for 10L$^\infty$. This difference is mostly a result of the application of updated equations of state and opacity tables; see the discussion comparing model 10H$^\infty$ with case J1 of Paper 1 presented in the text at the end of the previous section for additional details.

Table 3
Results

		10L$^{\infty}$	10L10	10L5	10L3	10H$^{\infty}$	10H10	10H5	6L$^{\infty}$	6L5	10V$^{\infty}$
First luminosity peak	Time[a]	0.29	0.29	0.26	0.23	0.33	0.33	0.28	0.47	0.47	0.30
	M_Z[b]	7.86	7.86	4.85	2.97	8.18	8.18	4.79	3.83	3.83	8.42
	M_{XY}[b]	0.013	0.013	0.0027	0.0007	0.007	0.007	0.001	0.003	0.003	0.015
	$\dot{M}_Z$	8.9×10^{-5}	8.9×10^{-5}	7.59×10^{-5}	4.9×10^{-5}	7.0×10^{-5}	7.0×10^{-5}	6.23×10^{-5}	1.87×10^{-5}	1.87×10^{-5}	8.1×10^{-5}
	$\langle \log L$[d]$\rangle$	−5.05	−5.05	−5.26	−5.57	−5.14	−5.14	−5.35	−5.94	−5.94	−5.07
End of Phase 1	Time[a]	0.38	0.32	0.26	0.23	0.45	0.36	0.28	0.65	0.55	0.39
	M_Z[b]	11.5	9.85	4.85	2.98	11.5	9.96	4.79	5.33	4.998	11.48
	M_{XY}[b]	0.31	0.038	0.0027	0.0007	0.21	0.019	0.001	0.087	0.016	0.29
	$\dot{M}_Z$[c]	8.8×10^{-6}	6.27×10^{-5}	7.59×10^{-5}	4.9×10^{-5}	3.5×10^{-6}	4.48×10^{-5}	6.23×10^{-5}	1.28×10^{-6}	8.1×10^{-6}	7.95×10^{-6}
	$\dot{M}_{XY}$[c]	8.8×10^{-6}	1.2×10^{-6}	1.6×10^{-7}	8.7×10^{-8}	3.5×10^{-6}	1.9×10^{-6}	3.9×10^{-8}	1.28×10^{-6}	3.3×10^{-7}	7.95×10^{-6}
	$\langle \log L$[d]$\rangle$	−5.89	−5.14	−5.26	−5.57	−6.27	−5.28	−5.37	−6.94	−6.22	−5.95
Mid-Phase 2	Time[a]	1.53	0.60	1.995	6.17	4.46	2.37	44.8	7.80	2.23	1.85
	M_Z[b]	14.0	10.0	5.0	3.0	14.0	10.0	5.051	6.51	5.0	14.0
	M_{XY}[b]	7.0	5.0	2.5	1.5	7.0	5.0	2.5	3.26	2.5	7.0
	$\dot{M}_Z$	2.25×10^{-6}	0	0	0	7.5×10^{-7}	0	0	1.57×10^{-7}	0	1.66×10^{-6}
	$\langle \dot{M}_{XY}$[c]$\rangle$	7.8×10^{-6}	1.94×10^{-5}	1.8×10^{-6}	5.5×10^{-7}	2.6×10^{-6}	2.68×10^{-6}	4.9×10^{-8}	5.6×10^{-7}	1.57×10^{-6}	5.88×10^{-6}
	$\langle \log L$[d]$\rangle$	−6.43	−6.77	−8.00	−8.8	−6.81	−7.18	−8.96	−7.75	−7.98	−6.53
Cross-over point	Time[a]	2.22	0.78	3.11	9.22	6.07	3.36	77.8	12.1	3.32	2.73
	$M_{\rm cross}$[b]	16.08	10.0	5.0	3.0	16.16	10.0	5.051	7.52	5.0	16.16
	$\langle \dot{M}_Z$[c]$\rangle$	4.0×10^{-6}	0	0	0	3.2×10^{-6}	0	0	3.6×10^{-7}	0	3.9×10^{-6}
	$\langle \dot{M}_{XY}$[c]$\rangle$	4.5×10^{-5}	4.4×10^{-5}	4.0×10^{-6}	1.3×10^{-6}	1.6×10^{-5}	9.5×10^{-6}	1.3×10^{-7}	1.82×10^{-6}	3.3×10^{-6}	1.9×10^{-5}
	$\langle \log L$[d]$\rangle$	−6.06	−6.44	−7.76	−8.45	−6.2	−6.64	−8.52	−7.37	−7.72	−6.20
Onset of limited gas accretion	Time[a]	2.28	0.91	4.46	11.89	6.33	3.83	95.25	13.23	4.656	2.87
	M_Z[b]	16.3	10.0	5.0	3.0	17.14	10.0	5.05	7.96	5.0	16.79
	M_{XY}[b]	47.24	38.76	50.83	59.21	45.40	45.8	31.36	43.74	47.67	46.24
	$\langle \log L$[d]$\rangle$	−4.38	−4.13	−4.41	−4.61	−3.96	−4.0	−4.29	−4.15	−4.62	−4.06

[a] Time is in units of millions of years, Myr.
[b] Mass is in units of Earth's mass, $M_{\oplus}$.
[c] The accretion rate is in units of Earth masses per year, $M_{\oplus}$/yr.
[d] Luminosity is in units of solar luminosity, $L_{\odot}$.

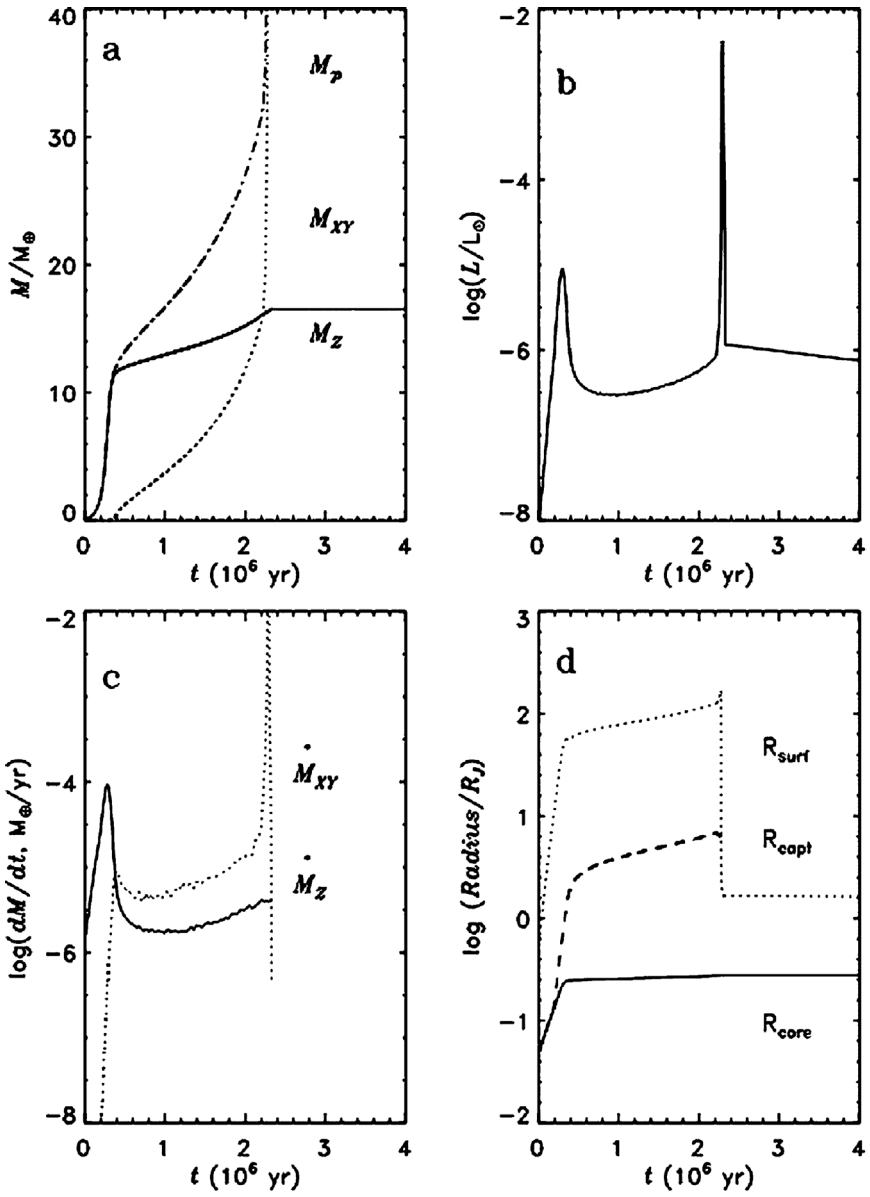

Fig. 1. Evolution of the baseline case, 10L$^\infty$, with $\sigma_{\mathrm{init},Z} = 10$ g/cm^2 and grain opacity at 2% interstellar value. (a) The mass is plotted as a function of time. The solid line denotes the solid core mass, M_Z, the dotted line denotes the envelope mass, M_{XY}, and the dash-dotted line denotes the total mass of the protoplanet, M_p. The value of M_p levels off at 1 M_J after 2.3 Myr, but the plot only displays masses up to the limit of $M_p = 40$ $M_\oplus$ in order to better display the crucial stages that are best simulated by our model. (b) The luminosity (in units of $L_\odot$) is plotted on a logarithmic scale as a function of time. (c) The solid line denotes the core accretion rate, $\dot{M}_Z$. The dotted line denotes the envelope accretion rate, $\dot{M}_{XY}$. (d) The radii plotted on a logarithmic scale as a function of time.

respectively, but is almost a factor of 10 less for 6L$^\infty$, $\log(L/L_\odot) = -5.95$. The maximum solid accretion rate is slightly higher for 10L$^\infty$ ($\dot{M}_Z = 9.1 \times 10^{-5}$ $M_\oplus$/yr) than for 10H$^\infty$ ($\dot{M}_Z = 7.3 \times 10^{-5}$ $M_\oplus$/yr). (The values of $\dot{M}_{Z,\max}$ are not presented in Table 3 but are very close to the values given for the First Luminosity Peak.) The M_Z at the end of Phase 1 for 6L$^\infty$ is 5.33 $M_\oplus$, which is in good agreement with the analytic isolation mass, 5.37 $M_\oplus$. (The models 10L$^\infty$ and 10V$^\infty$ will be discussed below.) The most notable differences in the "L$^\infty$" cases are apparent in Phase 2. Model 10L$^\infty$ evolves through Phase 2 quickly, reaching crossover in 2.22×10^6 yr with $M_{\mathrm{cross}} = 16.08$ $M_\oplus$. Model 6L$^\infty$ has a smaller crossover mass, 7.52 $M_\oplus$ and evolves more slowly, reaching crossover in 12.1×10^6 yr. The low grain opacity model allows a protoplanet to form quickly, a highly desirable result, and the low $\sigma_{\mathrm{init},Z}$ model forms a protoplanet with a low mass core, also a highly desirable result. However, to fit comfortably within the nominal constraints on the mass of Jupiter's core and lifetimes of observed protoplanetary disks, the requirement is to have these two results in the same model.

These cases clearly demonstrate the effect of the opacity on the formation time and the effect of solid surface density on the mass of the core. The duration of Phase 2 is the

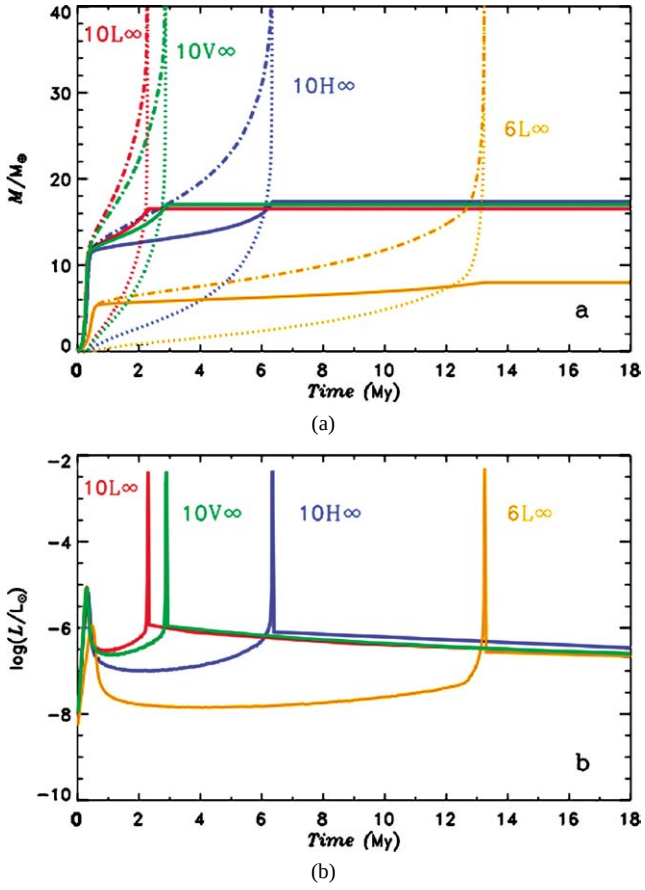

Fig. 2. Evolution of a giant protoplanet for several cases with no cutoff of the core mass. (a) The mass is plotted as a function of time. The solid lines denote M_Z, the dotted lines denote M_{XY}, and the dash-dotted lines denote the total mass. Red curves: model computed with $\sigma_{\mathrm{init},Z} = 10$ g/cm^2 and grain opacity values that are 2% interstellar. Green curves: $\sigma_{\mathrm{init},Z} = 10$ g/cm^2 and grain opacity at 2% interstellar value for $T < 350$ K and full interstellar at $T > 500$ K. Blue curves: $\sigma_{\mathrm{init},Z} = 10$ g/cm^2 and full interstellar grain opacity. Orange curves: $\sigma_{\mathrm{init},Z} = 6$ g/cm^2 and 2% interstellar grain opacity. As in Fig. 1a, the masses are plotted with the limit of $M_p = 40\ M_\oplus$ even though models are computed to $M = 1\ M_J$. The points where the curve reaches 40 $M_\oplus$ essentially give the formation times. (b) The luminosity as a function of time is plotted for the same cases.

main determinant of the formation time of the gas giant, and this time is determined by the sources and sinks of the thermal energy that keeps the massive envelope from collapsing. During most of Phase 2, the main source of energy comes from the accreting planetesimals, but the accretion rate is in turn controlled by the rate at which the envelope contracts (see Paper 1 for detailed discussion). As Phase 2 progresses, in the cases where there is no core accretion cutoff, the dominant energy source changes to the gravitational energy released from the outer envelope contraction which leads to gas accretion runaway. The opacity is an important quantity in governing the thermal response of the envelope. With low grain opacity in the envelope, more radiation escapes during Phase 2, thereby causing the envelope to contract faster, resulting in an increase in the gas accretion rate, causing crossover to occur quicker. When the solid surface density is reduced, the core accretion rate as well as the isolation mass become correspondingly less, and the envelope luminosity in Phase 2 is reduced (see Paper 1), resulting in slower contraction and a longer formation time.

The strong effect of grain opacity in the protoplanetary envelope on the evolution timescale is clearly demonstrated by cases 10L$^\infty$ and 10H$^\infty$. The time spent in Phase 2 is decreased by ∼70% when the grain opacity is 2% of the interstellar value. To further understand the effect of the grain opacity on the formation timescale, we computed case 10V$^\infty$, to examine if there was a particular temperature range over which the grain opacity was most influential. The grain opacity was set to 2% of the interstellar value for temperatures <350 K and to the full interstellar value for temperatures >500 K, with interpolation in the transition region. In the transition regime ($350 \leqslant T \leqslant 500$ K), the opacity values were linearly reduced. Fig. 2 shows that 10V$^\infty$ reduces the crossover time to 2.73 Myr from 6.07 Myr of case 10H$^\infty$, and it is very close to that of case 10L$^\infty$, 2.22 Myr. Clearly, the grain opacity effect is concentrated near the top of the envelope! This result is profoundly important, especially with reference to the grain settling work of Podolak (2003). The effects on the opacity of grain settling and coagulation will be examined more carefully in the future.

One of the underlying assumptions of our formation code is that the protoplanet evolved from a lone embryo orbiting the Sun. Most likely, there were many competing embryos, but our code does not compute the interaction of a multi-embryo system. However, we artificially simulate the result of this competition by turning off the solid accretion for specific core masses of the developing protoplanet, as if the remaining mass that would otherwise be available to the growing protoplanet were taken by the other competing protoplanets. We chose to recompute the later evolution of the three standard cases (10L$^\infty$, 10H$^\infty$, 6L$^\infty$) and stop the solid accretion at core masses of 10, 5, and 3 $M_\oplus$. The results of these runs are summarized in Table 3 and in Figs. 3, 4, and 5. The runs with stopped solid accretion are referred to as the cutoff runs.

Fig. 3 shows the mass and luminosity as a function of time for the simulation case 10L$^\infty$ and the corresponding cutoff runs 10L10, 10L5, and 10L3. Case 10L10 quickly evolved to crossover in 0.78×10^6 yr, whereas the run for which the cutoff occurs at 3 $M_\oplus$, 10L3, evolved the slowest, reaching crossover in 9.22×10^6 yr. The low core mass in 10L3 results in a significant interval of time between crossover and limiting gas accretion, which is reached at 11.89×10^6 yr. Case 10L5 reached crossover in 3.11×10^6 yr, almost a million years longer than the baseline run, 10L$^\infty$. The luminosity as a function of time is plotted in Fig. 3b; this plot shows that all the cutoff runs dip below the minimum luminosity of the baseline case, but after a short amount of time 10L10 quickly increases in luminosity.

The masses of the components of the planet as functions of time for the simulations with the grain opacity at

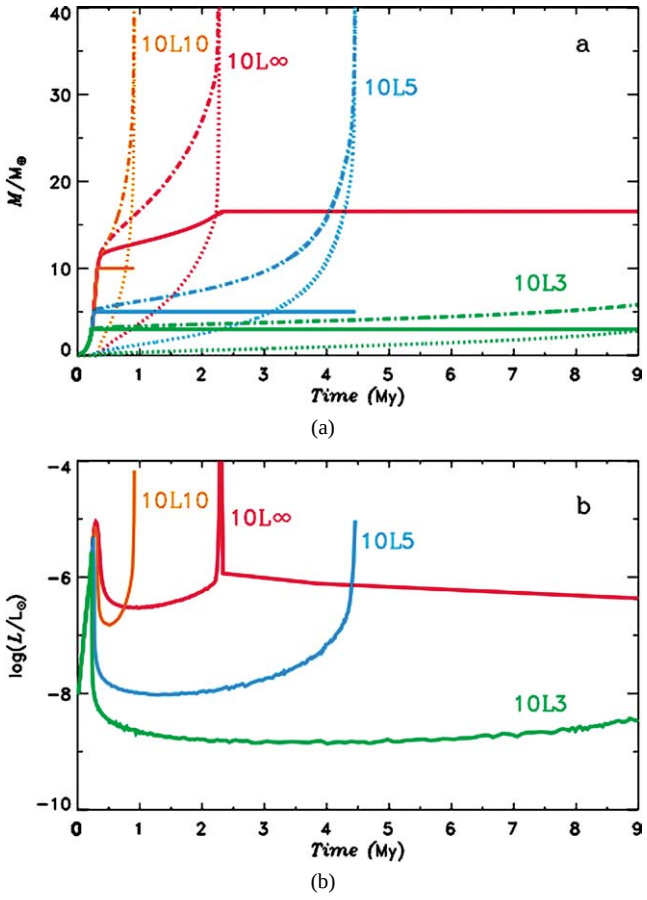

Fig. 3. Evolution of a giant protoplanet with $\sigma_{\text{init},Z} = 10$ g/cm^2 and grain opacity at 2% interstellar value. (a) The mass is plotted as a function of time with the same line denotation as in Figs. 1 and 2. Red curves: no solid accretion cutoff. Orange curves: solid accretion cutoff at 10 $M_\oplus$. Blue curves: solid accretion cutoff at 5 $M_\oplus$. Green curves: solid accretion cutoff at 3 $M_\oplus$. (b) The luminosity is plotted on a logarithmic scale as a function of time. Note that the cutoff runs are halted when the gas accretion rate reaches a limiting value defined by the rate at which the solar nebula can transport gas to the vicinity of the planet, whereas the planet in the run with no cutoff stops growing when $M_p = 1\ M_J$.

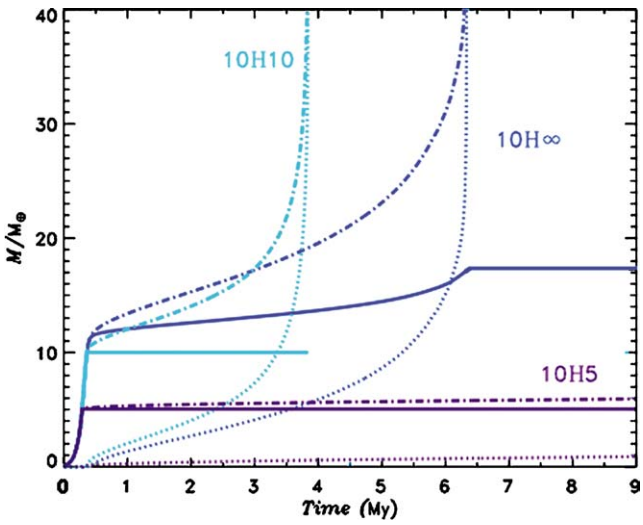

Fig. 4. Evolution of a giant protoplanet with $\sigma_{\text{init},Z} = 10$ g/cm^2 and full interstellar grain opacity. The mass is plotted as a function of time, with the same line style denotation as in previous figures. Blue curves: no solid accretion cutoff. Light blue curves: solid accretion cutoff at 10 $M_\oplus$. Purple curves: solid accretion cutoff at 5 $M_\oplus$. This plot is analogous to Fig. 3a.

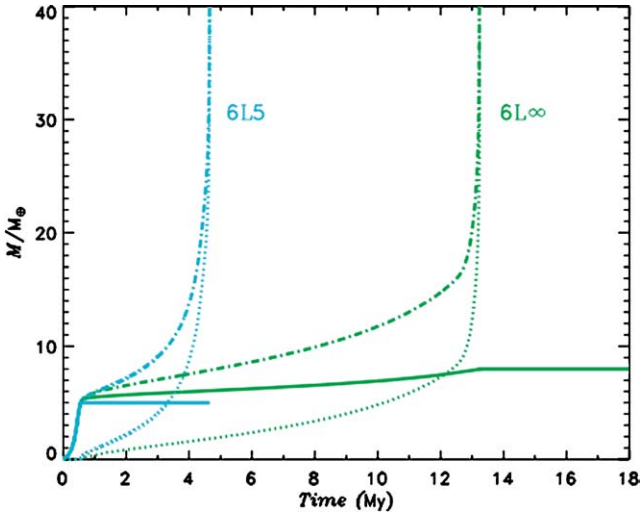

Fig. 5. Evolution of a giant protoplanet with $\sigma_{\text{init},Z} = 6$ g/cm^2 and grain opacity at 2% interstellar value. Green curves: no solid accretion cutoff. Light green curves: solid accretion cutoff at 5 $M_\oplus$. See caption to Fig. 3 for other details.

full interstellar value, the 10H runs, is shown in Fig. 4. Case 10H10 quickly evolved through Phase 2 to crossover in 3.36×10^6 yr, which is about half the time of 10H$^\infty$. However, case 10H5 required an unexpectedly long evolution time; it took the simulated protoplanet 77.8×10^6 yr to reach crossover. Since 10H5 model took a long time to evolve, we saw no reason to compute a cutoff run with a 3 $M_\oplus$ core. Though not shown, the luminosity for the three 10H runs follows similar trends as the 10L runs in Fig. 3, with 10H10 exhibiting an increase in luminosity after taking a dip below that of 10H$^\infty$. The mass as a function of time for the 6L runs is plotted in Fig. 5. The evolution time to crossover for model 6L5, 3.32×10^6 yr, is significantly less than the 6L$^\infty$ time of 12.1×10^6 yr and only slightly longer than the 10L5 time of 3.11×10^6 yr.

These cutoff runs demonstrate that a gas runaway occurs earlier than for the baseline case as long as the cutoff occurs near the isolation mass. The reason for this is connected with the energy source. Without a cutoff, during Phase 2, planetesimal accretion dominates the energy production. If that source is cutoff just before Phase 2, the envelope must contract fairly rapidly to provide for its radiated luminosity. Therefore, the rate of inflow of the gas from the nebula increases, and crossover occurs earlier. On the other hand, if the cutoff occurs with a core mass significantly lower than the isolation mass, the luminosity radiated by the envelope, which, during most of Phase 2, goes as the 4th power of the core mass (Paper 1), is significantly reduced. Thus, the envelope contracts slowly and the timescale for the gas accretion becomes longer. The effect of the mass-luminosity relation

on increasing the timescale for gas accretion is more important than the effect of the lack of planetesimal accretion on reducing that timescale in this case.

4. Summary and conclusion

The simulations of this study demonstrate that the atmospheric opacity due to grains plays a significant role in determining the temporal and physical nature of the evolution of a gas giant protoplanet. Of comparable importance to the formation of a gas giant planet is the mass of the solid core when the solid matter ceases to be accreted. The approach that we took by using a cutoff core mass is a relatively easy parameterization that examines the effect of competing embryos; but it is a gross simplification, and in future work we will apply more realistic planetesimal scenarios that explicitly take into account a distribution in planetesimal size and growth rates (e.g., Weidenschilling et al., 1997). Opacity is an even more complicated issue. Podolak (2003) has recently undertaken the task of explicitly examining the effect on the grain opacity of the settling, coagulation, and evaporation of grains in a protoplanetary envelope, both those provided by the inflow of gas from the nebula and those ablated from infalling planetesimals.

Typical protoplanetary envelope opacity profiles are illustrated in Fig. 6. The opacity as a function of temperature is plotted for the three $\sigma_{\text{init},Z} = 10$ g/cm^2 cases at mid-phase 2: 10L$^\infty$, 10H$^\infty$, and 10V$^\infty$. The opacity of the envelope is dominated by the grain opacity for $T < 1800$ K and it is relatively constant, $\sim$0.03 cm^2/g for 10L$^\infty$ and $\sim$2 cm^2/g

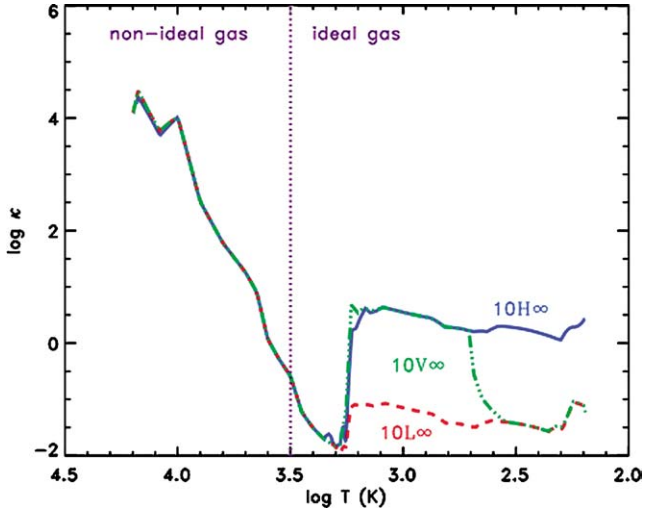

Fig. 6. The logarithm of the opacity (units of cm^2/g) is plotted as a function of temperature for models at mid-Phase 2, which occurs at $M_Z = 14.0\ M_\oplus$ and $M_{XY} = 7.0\ M_\oplus$ for the 10–$^\infty$ runs that are represented in this figure. Red curve: models computed with $\sigma_{\text{init},Z} = 10$ g/cm^2 and grain opacity values that are 2% interstellar. Green curve: $\sigma_{\text{init},Z} = 10$ g/cm^2 and grain opacity at 2% of interstellar value for $T < 350$ K and full interstellar at $T > 500$ K. Blue curve: $\sigma_{\text{init},Z} = 10$ g/cm^2 and full interstellar grain opacity.

for 10H$^\infty$. The profile for 10V$^\infty$ has the opacity value of 10L$^\infty$ near the surface and follows the opacity of 10H$^\infty$ in the lower part of the envelope. Examination of Fig. 2 and the values in Table 3 for 10L$^\infty$ and 10V$^\infty$ indicates that there is very little difference between these two cases at the five salient times of the evolution, and we conclude that the difference in the overall results between 10L$^\infty$ and 10H$^\infty$ is primarily due to the lower grain opacity in the uppermost region of the envelope, where $T \leqslant 500$ K. Following this trend of our results, the effect of further lowering the opacity in the outermost and least dense upper region of the envelope should be to further decrease the formation time of the gas giant planet.

The effect of grain opacity and core mass on the formation time of giant planets was examined by INE00. Making a direct comparison of the INE00 results with this study is not straightforward because of some fundamental differences in the simulation input parameters. Most notable is the use of a constant grain opacity as a parameter in their models, whereas we apply the opacity tables of Pollack et al. (1985) and Alexander and Ferguson (1994). INE00 use a constant solid accretion rate as an input parameter in their computations, whereas in our study the rate is based on the gravitational enhancement factor for three-body growth rates computed by Greenzweig and Lissauer (1992). Thus their models do not show a Phase 2. Our energy profile includes considerations involving the vaporization of water ice, CHON, and rock materials ablated from the accreted planetesimals. The density of the core in our models is 3.2 g/cm^3, and they use 5.5 g/cm^3. Finally, our definition for the onset of gas runaway is different from that used in the INE00 models. They define M_{crit} to be the mass of the core of the protoplanet above which a model in strict hydrostatic equilibrium cannot be computed. Our criterion is based on M_{cross}, which is defined as the point where gas and solid masses in the protoplanet are equal. However, because of the relative constancy of the accretion rates in Phase 2 in our models, we will compare the trends in our results with those in the results of INE00, which, in general are qualitatively similar.

The focus of the comparison of our results with those of INE00 is the effects of κ_{gr}, M_{core}, and $\sigma_{\text{init},Z}$ on the growth times of the protoplanet. For a constant κ_{gr}, the overall trend is that the formation time increases with decreasing M_{core}. Increasing M_{core} from 5 to 10 $M_\oplus$ at $\kappa_{\text{gr}} = 1$ cm^2/g, the INE00 models with core accretion cutoff show a decrease in the formation time by 92%, from 3.5×10^6 to 2.5×10^5 yr. In our study, comparing cases 10H5 and 10H10, there is a 96% decrease in the time to t_{cross}, from 77.8×10^6 to 3.36×10^6 yr. For the 10L cases, comparing 10L5 and 10L10, the reduction in time is 75%, from 3.11×10^6 to 0.78×10^6 yr. For a particular M_{core}, a decrease in the opacity causes a steep decrease in the formation time. Particular values for 3 $M_\oplus$ are given by INE00: reducing κ_{gr} from 1.0 to 0.01 cm^2/g, the formation time drops from 12×10^6 to 0.15×10^6 yr, a 98% decrease. We do not have data to com-

pare at 3 $M_\oplus$, but with core mass cutoff at 5 $M_\oplus$ for cases 10H5 and 10L5, where there is a factor of fifty difference in opacity (i.e., roughly 2–0.04 cm^2/g; see Fig. 6), $t_{\rm cross}$ decreases from 77.8×10^6 to 3.11×10^6 yr, a 96% reduction. At 10 $M_\oplus$, our data show a less steep decrease because $t_{\rm cross}$ goes from 3.36×10^6 to 0.78×10^6 yr, a 77% decrease. Clearly, the magnitude of the values differ, but the effect of the parameters on the formation time scale is qualitatively similar. A rough comparison of no cutoff (infinity) cases vs cutoff cases is also possible. Using a core accretion rate of 10^{-6} $M_\oplus$/yr and a constant grain opacity of 1 cm^2/g, their core mass is 11 $M_\oplus$ and the characteristic growth time of the envelope is 10^6 yr with no core accretion cutoff. With cutoff at the same core mass their growth time is 2×10^5 yr, a factor 5 shorter. These parameters are approximately the same as we use in the cases 10H$^\infty$ and 10H10, where we obtain a ratio of envelope accretion times, without and with cutoff, of about a factor of 2.

Although there are some differences between our results and theirs, because of different approximations and assumptions, our overall conclusion is quite similar to that of INE00: In order to form Jupiter by core accretion at 5 AU in a time of 10^7 yr or less, a solid surface density of approximately 3–4 times that of the minimum mass solar nebula is needed if the atmospheric opacity is similar to that of interstellar matter, twice this minimum surface density and a low opacity (6L5 case) is also sufficient; a substantial reduction in grain opacity results in shorter formation times.

The goal of this paper is to show under what conditions a planet of Jupiter's mass can form with a core mass of 5–10 $M_\oplus$ in a few (2–5) Myr. Fig. 7 is a plot of the core mass at the time of the onset of limited gas accretion as a function of the accretion time for all our models. The limits on mass and time deduced from observations and interior models are marked and labeled. One model (10H5) is not plotted because its accretion time (95.25 Myr) is outside the scope of the plot limits. If erosion of the core and mixing of its material with that of the envelope occurs at times following the formation phase (Stevenson, 1982; Guillot, 2001), then our results may also be applicable to gas giant planets with smaller or no cores, provided their total heavy element inventories are at least 5–10 $M_\oplus$. Our conclusions can be summarized as follows: (1) In cases where the opacity of the atmosphere is equal to that of typical interstellar material (10H series), it is not possible to satisfy both small core size and rapid formation time simultaneously. (2) An entirely reasonable reduction in the grain opacity below interstellar values results in a speedup in the formation time, but it does not affect the final core mass. (3) In our baseline case (10L$^\infty$), we find that Jupiter can be formed at 5 AU in a time of just over 2 Myr, but the core mass is 16 $M_\oplus$. (4) If accretion stops when the core mass has reached the range 5–10 $M_\oplus$, and if the initial solid surface density in the disk is 3 times that of the minimum mass solar nebula, formation times fall in the range 1–4.5 Myr and the core mass is consistent with observations of Jupiter. (5) If

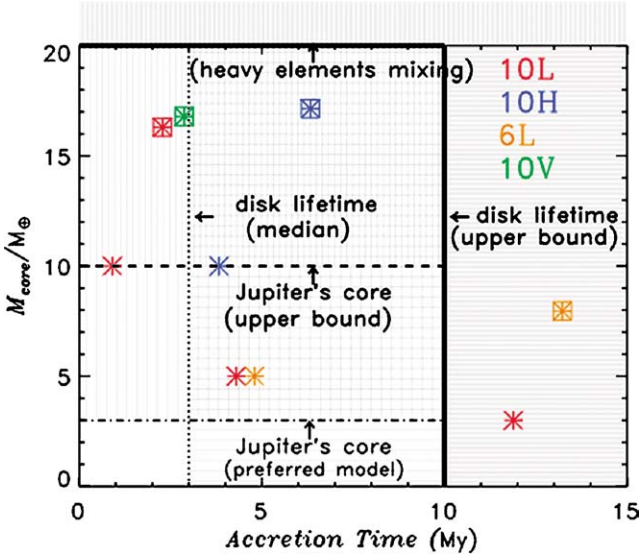

Fig. 7. The core mass as a function of the time at the onset of runaway gas accretion for the four series of computed models. Red symbols denote models computed with $\sigma_{{\rm init},Z} = 10$ g/cm^2 and grain opacity values that are 2% interstellar. Blue symbols denote models computed with $\sigma_{{\rm init},Z} = 10$ g/cm^2 and full interstellar grain opacity. Orange symbols denote models computed with $\sigma_{{\rm init},Z} = 6$ g/cm^2 and 2% interstellar grain opacity. Green symbols denote models computed with $\sigma_{{\rm init},Z} = 10$ g/cm^2 and grain opacity at 2% of interstellar value for $T \leqslant 350$ K and full interstellar at $T > 500$ K. One model (10H5 with $M_{\rm core} = 5\ M_J$ and $T_{\rm acc} = 95.25$ Myr) is not plotted because it is outside the scope of the plot's limit. The *boxed symbols* denote the models for which there is *no* solid accretion cutoff; the mass at which the other runs are cut off is given by their vertical coordinate on the plot. The *solid vertical line* represents the approximate maximum observed disk lifetime around young stars. The *dotted line* represents the median observed disk lifetime. The *dot-dash* and the *dashed lines* represent, respectively, the preferred and the maximum value of Jupiter core mass, obtained from comparison of theoretical models with observations. The *bold* horizontal line at 20 $M_\oplus$, labeled "heavy elements mixing," represents a possible primordial core mass for Jupiter which was later eroded by convective mixing of heavy elements into the gaseous envelope. Regions above and to the right of the bold solid lines are strongly excluded by observations. Those failing less certain observational limits appear as partially shaded.

the initial solid surface density in the disk is reduced to 2 times that of the minimum mass solar nebula, it is still possible to form Jupiter in less than 5 Myr if the core accretion is cut off at 5 $M_\oplus$. (6) If the actual core mass of Jupiter is only 3 $M_\oplus$ (Saumon and Guillot, 2004), a result still subject to major observational, experimental, and theoretical uncertainty, then the problem remains whether the planet can form in 3 Myr or less. This problem could be solved in one or more of the following three ways: first, by core erosion after formation, as mentioned above, second, by taking into account in the models, the fact that some of the arriving planetesimals do not sink to the core but instead are dissolved in the envelope, or third, by the atmospheric opacity being significantly less than 2% that of the interstellar medium. (7) All models presented herein satisfy the constraint that the total heavy element abundance is less than or comparable to the value deduced from observations of Jupiter. A few

models have low heavy element abundance (3–5 $M_\oplus$), but it is quite reasonable to expect the planet to accrete more solids during or after rapid gas accretion, which is not taken into account in these models. (8) The results of Pollack et al. (1996) showed that Phase 2, the early gas accretion phase before crossover mass is reached, determined the timescale for formation of a giant planet. However, the present results indicate that for low atmospheric opacity and/or a cutoff in accretion of solids Phase 2 can be relatively short, and the time for Phase 1, the solid core accretion phase, may be the determining factor. Note, however, that Pollack et al. (1996) showed that for the case of Uranus, the duration of Phase 1 was reduced by a factor of 15 when the planetesimal size of 1 km was used rather than the standard value of 100 km. (9) Recent simulations of the core accretion process, taking into account multiple embryos and a number of other physical processes (Inaba et al., 2003; Thommes et al., 2003; Kokubo and Ida, 2002), indicate that core formation times may be longer than those computed here. Thus, the question remains as to how large an enhancement of solid surface density, as compared with that in the minimum mass solar nebula, is needed to form a giant planet in a few Myr. That question, in connection with an improved estimate of the solid accretion rate during Phase 1, will be examined in the future.

This work, although focused on Jupiter, can be extended in the future to include Saturn and the extrasolar planets. In the case of Saturn, the timescale to build a core of $\sim$15 $M_\oplus$ will be the primary problem (Inaba et al., 2003). The accretion time for the gas around a core of that mass should be less than 2 Myr, as in the baseline case of this paper. For extrasolar planets, the core accretion model preferentially forms planets at distances of 4–20 AU from a 1 solar mass star (Lissauer, 1987; Paper 1, Kornet et al., 2005). It is very difficult to form jovian planets close to the star (BHL, 2000), so the extrasolar planets interior to $\sim$2 AU almost certainly arrived there by migration (Goldreich and Tremaine, 1979; Lin et al., 1996).

Acknowledgments

We acknowledge very helpful remarks by reviewer Alan Boss, by an anonymous second referee, and especially Kevin Zahnle for carefully reading the manuscript and making many helpful suggestions. O.H. and P.B. were supported in part by NASA Grant NAG 5-9661 and NASA Grant NAG 5-13285 from the Origins of Solar Systems Program. J.J.L. received support from NASA's Outer Planets Research Program Grant 344-30-99-02.

References

Alibert, Y., Mordasini, C., Benz, W., 2004. Migration and giant planet formation. Astron. Astrophys. 417, L25–L28.

Alibert, Y., Mordasini, C., Benz, W., Winisdoerffer, C., 2005. Models of giant planet formation with migration and disk evolution. Astron. Astrophys. 434, 343–353.

Alexander, D.R., 1975. Low-temperature Rosseland opacity tables. Astrophys. J. Suppl. 29, 363–374.

Alexander, D.R., Ferguson, J.W., 1994. Low-temperature Rosseland opacities. Astrophys. J. 437, 879–891.

Alexander, D.R., Johnson, H.R., Rypma, R.L., 1983. Effect of molecules and grains on Rosseland mean opacities. Astrophys. J. 272, 773–780.

Bodenheimer, P., Pollack, J.B., 1986. Calculations of the accretion and evolution of giant planets: The effects of solid cores. Icarus 67, 391–408 (BP86).

Bodenheimer, P., Lin, D.N.C., 2002. Implications of extrasolar planets for understanding planet formation. Annu. Rev. Earth Planet. Sci. 30, 113–148.

Bodenheimer, P., Hubickyj, O., Lissauer, J.J., 2000. Models of the in situ formation of detected extrasolar giant planets. Icarus 143, 2–14 (BHL00).

Boss, A.P., 1998. Evolution of the solar nebula. IV. Giant gaseous protoplanet formation. Astrophys. J. 503, 923–937.

Boss, A.P., 2000. Possible rapid gas giant planet formation in the solar nebula and other protoplanetary disks. Astrophys. J. 536, L101–L104.

Boss, A.P., 2003. Rapid formation of outer giant planets by disk instability. Astrophys. J. 599, 577–581.

Boss, A.P., 2004. Convective cooling of protoplanetary disks and rapid giant planet formation. Astrophys. J. 610, 456–463.

Bouwmann, J., Meyer, M., 2005. Formation and evolution of planetary systems—Placing our Solar System in context. In: Proceedings of the Meeting: Ringberg Workshop on Planet Formation. Rinberg Castle, Bavaria. December 19–22, 2004. In press.

Bryden, G., Chen, X., Lin, D.N.C., Nelson, R.P., Papaloizou, J.C.B., 1999. Tidally induced gap formation in protostellar disks: Gap clearing and suppression of protoplanetary growth. Astrophys. J. 514, 344–367.

Cai, K., Durisen, R.H., Mejía, A.C., 2004. Boundary conditions of radiative cooling in gravitationally unstable protoplanetary disks. In: American Astronomical Society 204th Meeting. Abstract 62.19.

Cameron, A.G.W., 1978. Physics of the primitive solar accretion disk. Moon Planets 18, 5–40.

Chen, C.H., Kamp, I., 2004. Are giant planets forming around HR 4796A? Astrophys J. 602, 985–992.

Cox, A.N., Stewart, J.N., 1970. Rosseland opacity tables for population I compositions. Astrophys. J. Suppl. 19, 243–259.

D'Angelo, G., Henning, T., Kley, W., 2003. Thermodynamics of circumstellar disks with high-mass planets. Astrophys. J. 599, 548–576.

DeCampli, W.M., Cameron, A.G.W., 1979. Structure and evolution of isolated giant gaseous protoplanets. Icarus 38, 367–391.

Descartes, R., 1644. Principia Philosophiae. Elzevir, Amsterdam. In Latin.

Fischer, D.A., Valenti, J.A., 2003. Metallicities of stars with extrasolar planets. In: Deming, D., Seager, S. (Eds.), Scientific Frontiers in Research on Extrasolar Planets. In: ASP Conference Series, vol. 294. Astronomical Society of the Pacific, San Francisco, pp. 117–128.

Fischer, D.A., Valenti, J.A., 2005. The planet-metallicity correlation. Astrophys. J. 622, 1102–1117.

Gammie, C.F., 2001. Nonlinear outcome of gravitational instability in cooling, gaseous disks. Astrophys. J. 553, 174–183.

Goldreich, P., Tremaine, S., 1979. The excitation of density waves at the Lindblad and corotation resonances by an external potential. Astrophys. J. 233, 857–871.

Gonzalez, G., 1998. Spectroscopic analyses of the parent stars of extrasolar planetary system candidates. Astron. Astrophys. 334, 221–238.

Graboske Jr., H.C., Olness, R.J., Grossman, A.S., 1975. Thermodynamics of dense hydrogen–helium fluids. Astrophys. J. 199, 255–264.

Greenberg, R., Wacker, J.F., Hartman, W.K., Chapman, C.R., 1978. Planetesimals to planets: Numerical simulations of collisional evolution. Icarus 35, 1–26.

Greenzweig, Y., Lissauer, J.J., 1992. Accretion rates of protoplanets. II. Gaussian distributions of planetesimal velocities. Icarus 100, 440–463.

Grossman, A.S., Pollack, J.B., Reynolds, R.T., Summers Jr., A.L., Graboske, H.C., 1980. The effect of dense cores on the structure and evolution of Jupiter and Saturn. Icarus 42, 358–379.

Guillot, T., 2001. Mixing the cores and envelopes of the giant planets: Consequences for formation models. In: American Astronomical Society, DPS Meeting 33. Abstract 23.06.

Guillot, T., 2005. The interiors of giant planets: Models and outstanding questions. Annu. Rev. Earth Planet. Sci. 33, 493–530.

Guillot, T., Gautier, D., Hubbard, W.B., 1997. New constraints on the composition of Jupiter from Galileo measurements and interior models. Icarus 130, 534–539.

Guillot, T., Stevenson, D.J., Hubbard, W.B., Saumon, D., 2004. The interior of Jupiter. In: Bagenal, F., Dowling, T.E., McKinnon, W.B. (Eds.), Jupiter: The planet, satellites, and magnetosphere. Cambridge Univ. Press, Cambridge, pp. 35–57.

Haisch Jr., K.E., Lada, E.A., Lada, C.J., 2001. Disk frequencies and lifetimes in young clusters. Astrophys. J. 553, L153–L156.

Hollenbach, D.J., Yorke, H.W., Johnstone, D., 2000. Disk dispersal around young stars. In: Mannings, V., Boss, A.P., Russell, S. (Eds.), Protostars and Planets IV. Univ. of Arizona Press, Tucson, pp. 401–428.

Ida, S., Lin, D.N.C., 2004. Toward a deterministic model of planetary formation. II. The formation and retention of gas giant planets around stars with a range of metallicities. Astrophys. J. 616, 567–572.

Ikoma, M., Nakazawa, K., Emori, H., 2000. Formation of giant planets: Dependences on core accretion rate and grain opacity. Astrophys. J. 537, 1013–1025 (INE00).

Inaba, S., Wetherill, G.W., Ikoma, M., 2003. Formation of gas giant planets: Core accretion models with fragmentation and planetary envelope. Icarus 166, 46–62.

Kant, I., 1755. Allgemeine Naturgeschichte und Theorie des Himmels. Johann Friederich Petersen, Koenigsberg/Leipzig.

Kary, D.M., Lissauer, J.J., 1994. Numerical simulations of planetary growth. In: Franco, J., Lizano, S., Aguilar, E., Daltabuit, L. (Eds.), Numerical Simulations in Astrophysics. Cambridge Univ. Press, Cambridge, pp. 364–373.

Kley, W., 1999. Mass flow and accretion through gaps in accretion discs. Mon. Not. R. Astron. Soc. 303, 696–710.

Kley, W., D'Angelo, G., Henning, T., 2001. Three-dimensional simulations of a planet embedded in a protoplanetary disk. Astrophys. J. 547, 457–464.

Kokubo, E., Ida, S., 2002. Formation of protoplanet systems and diversity of planetary systems. Astrophys. J. 581, 666–680.

Kornet, K., Bodenheimer, P., Różyczka, M., Stepinski, T.F., 2005. Formation of giant planets in disks with different metallicities. Astron. Astrophys. 430, 1133–1138.

Kuiper, G.P., 1951. On the origin of the Solar System. In: Hynek, J.A. (Ed.), Astrophysics. McGraw–Hill, New York, pp. 357–424.

Laplace, P.S., 1796. Exposition de Système du Monde. Circle-Sociale, Paris. English translation: H.H. Harte, 1830. The System of the World. Dublin Univ. Press, Dublin.

Lin, D.N.C., Bodenheimer, P., Richardson, D., 1996. Orbital migration of the planetary companion of 51 Pegasi to its present location. Nature 380, 606–607.

Lissauer, J.J., 1987. Timescales for planetary accretion and the structure of the protoplanetary disk. Icarus 69, 249–265.

Lissauer, J.J., Pollack, J.B., Wetherill, G.W., Stevenson, D.J., 1995. Formation of the Neptune system. In: Cruikshank, D., Matthews, M.S., Schumann, A.M. (Eds.), Neptune and Triton. Univ. of Arizona Press, Tucson, pp. 37–108.

Livio, M., Pringle, J.E., 2003. Metallicity, planetary formation, and migration. Mon. Not. R. Astron. Soc. 346, L42–L44.

Lubow, S.H., Seibert, M., Artymowicz, P., 1999. Disk accretion onto high-mass planets. Astrophys. J. 525, 1001–1012.

Marley, M.S., 1999. Interiors of the giant planets. In: Weissman, P., McFadden, L.A., Johnson, T.V. (Eds.), Encyclopedia of the Solar System. Academic Press, New York, pp. 339–355.

Mayer, L., Quinn, T., Wadsley, J., Stadel, J., 2002. Formation of giant planets by fragmentation of protoplanetary disks. Science 298, 1756–1759.

Mayer, L., Quinn, T., Wadsley, J., Stadel, J., 2004. The evolution of gravitationally unstable protoplanetary disks: Fragmentation and possible giant planet formation. Astrophys. J. 609, 1045–1064.

Mejía, A.C., Durisen, R.H., Pickett, M.K., Cai, K., 2005. The thermal regulation of gravitational instabilities in protoplanetary disks. II. Extended simulations with varied cooling rates. Astrophys. J. 619, 1098–1113.

Mizuno, H., 1980. Formation of the giant planets. Prog. Theor. Phys. 64, 544–557.

Mizuno, H., Nakazawa, K., Hayashi, C., 1978. Instability of a gaseous envelope surrounding a planetary core and formation of giant planets. Prog. Theor. Phys. 60, 699–710.

Nelson, R.P., Papaloizou, J.C.B., Masset, F., Kley, W., 2000. The migration and growth of protoplanets in protostellar discs. Mon. Not. R. Astron. Soc. 318, 18–36.

Owen, T., Mahaffy, P., Nieman, H.B., Atreya, S., Donahue, T., Bar-Nun, A., de Pater, I., 1999. A low-temperature origin for the planetesimals that formed Jupiter. Nature 402, 269–270.

Papaloizou, J.C.B., Nelson, R.P., 2005. Models of accreting gas giant protoplanets in protostellar disks. Astron. Astrophys. 433, 247–265.

Perri, F., Cameron, A.G.W., 1974. Hydrodynamic instability of the solar nebula in the presence of a planetary core. Icarus 22, 416–425.

Pickett, B.K., Mejía, A.C.R., Durisen, H., Cassen, P.M., Berry, D.K., Link, R.P., 2003. The thermal regulation of gravitational instabilities in protoplanetary disks. Astrophys. J. 590, 1060–1080.

Podolak, M., 2003. The contribution of small grains to the opacity of protoplanetary atmospheres. Icarus 165, 428–437.

Podolak, M., Pollack, J.B., Reynolds, R.T., 1988. Interactions of planetesimals with protoplanetary atmospheres. Icarus 73, 163–179.

Pollack, J.B., 1985. Formation of the giant planets and their satellite–ring systems: An overview. In: Black, D.C., Matthews, M.S. (Eds.), Protostars and Planets II. Univ. of Arizona Press, Tucson, pp. 791–831.

Pollack, J.B., Bodenheimer, P., 1989. Theories of the origin and evolution of the giant planets. In: Atreya, S.K., Pollack, J.B., Matthews, M.S. (Eds.), Origin and Evolution of Planetary and Satellite Atmospheres. Univ. of Arizona Press, Tucson, pp. 564–604.

Pollack, J.B., McKay, C.P., Christofferson, B., 1985. A calculation of the Rosseland mean opacity of dust grains in primordial Solar System nebulae. Icarus 64, 471–492.

Pollack, J.B., Hubickyj, O., Bodenheimer, P., Lissauer, J.J., Podolak, M., Greenzweig, Y., 1996. Formation of the giant planets by concurrent accretion of solids and gas (Paper 1). Icarus 124, 62–85.

Rafikov, R.R., 2005. Can giant planets form by direct gravitational instability? Astrophys. J. 621, L69–L72.

Rice, W.K.M., Armitage, P.J., 2003. On the formation time scale and core masses of gas giant planets. Astrophys. J. 598, L55–L58.

Rice, W.K.M., Armitage, P.J., Bate, M.R., Bonnell, I.A., 2003a. The effect of cooling on the global stability of self-gravitating protoplanetary discs. Mon. Not. R. Astron. Soc. 339, 1025–1030.

Rice, W.K.M., Armitage, P.J., Bonnell, I.A., Bate, M.R., Jeffers, S.V., Vine, S.G., 2003b. Substellar companions and isolated planetary-mass objects from protostellar disc fragmentation. Mon. Not. R. Astron. Soc. 346, L36–L40.

Safronov, V.S., 1969. Evolution of the Protoplanetary Cloud and Formation of the Earth and Planets. Nauka, Moscow. In Russian, English translation: NASA-TTF-677, 1972.

Santos, N.C., Israelian, G., Mayor, M., 2001. The metal-rich nature of stars with planets. Astron. Astrophys. 373, 1019–1031.

Santos, N.C., Israelian, G., Mayor, M., Rebolo, R., Udry, S., 2003. Statistical properties of exoplanets. II. Metallicity, orbital parameters, and space velocities. Astron. Astrophys. 398, 363–376.

Santos, N.C., Israelian, G., Mayor, M., 2004. Spectroscopic [Fe/H] for 98 extra–solar planet–host stars: Exploring the probability of planet formation. Astron. Astrophys. 415, 1153–1166.

Saumon, D., Guillot, T., 2004. Shock compression of deuterium and the interiors of Jupiter and Saturn. Astrophys. J. 609, 1170–1180.

Saumon, D., Chabrier, G., Van Horn, H.M., 1995. An equation of state for low-mass stars and giant planets. Astrophys. J. Suppl. 99, 713–741.

Sigurdsson, S., Richter, H.B., Hansen, B.M., Stairs, I.H., Thorsett, S.E., 2003. A young white dwarf companion to pulsar B1620–26: Evidence for early planet formation. Science 301, 193–196.

Sozzetti, A., 2004. On the correlation between the orbital periods of extrasolar planets and the metallicity of the host stars. Mon. Not. R. Astron. Soc. 354, 1194–1200.

Stevenson, D.J., 1982. Formation of the giant planets. Planet Space Sci. 30, 755–764.

Strom, S.E., Edwards, S., Skrutskie, M.F., 1993. Evolutionary time scales for circumstellar disks associated with intermediate- and solar-type stars. In: Levy, E.H., Lunine, J.I. (Eds.), Protostars and Planets III. Univ. of Arizona Press, Tucson, pp. 837–866.

Tanaka, H., Takeuchi, T., Ward, W.R., 2002. Three-dimensional interaction between a planet and an isothermal gaseous disk. I. Corotation and Lindblad torques and planet migration. Astrophys. J. 565, 1257–1274.

Tajima, N., Nakagawa, Y., 1997. Evolution and dynamical stability of the proto-giant-planet envelopes. Icarus 126, 282–292.

Thommes, E.W., Duncan, M.J., Levison, H.F., 2003. Oligarchic growth of giant planets. Icarus 161, 431–455.

Toomre, A., 1964. On the gravitational stability of a disk of stars. Astrophys. J. 139, 1217–1238.

Weidenschilling, S.J., 1977. The distribution of mass in the planetary system and solar nebula. Astrophys. Space Sci. 51, 153–158.

Weidenschilling, S.J., Spaute, D., Davis, D.R., Marzari, F., Ohtsuki, K., 1997. Accretional evolution of a planetesimal swarm. 2. The terrestrial zone. Icarus 128, 429–455.

Wuchterl, G., Guillot, T., Lissauer, J.J., 2000. Giant planet formation. In: Mannings, V., Boss, A.P., Russell, S. (Eds.), Protostars and Planets IV. Univ. of Arizona Press, Tucson, pp. 1081–1109.

Young, R.E., 2003. The Galileo probe: How it has changed our understanding of Jupiter. New Astron. Rev. 47, 1–51.